Published in final edited form as:

Nat Chem Biol. 2016 October ; 12(10): 795–801. doi:10.1038/nchembio.2131.

Inhibiting androgen receptor nuclear entry in castration-resistant prostate cancer

Julie A. Pollock[1,5,6], **Suzanne E. Wardell**[2,6], **Alexander A. Parent**[1,6], **David B. Stagg**[2], **Stephanie J. Ellison**[2], **Holly M. Alley**[2], **Christina A. Chao**[2], **Scott A. Lawrence**[2], **James P. Stice**[2], **Ivan Spasojevic**[3,4], **Jennifer G. Baker**[2], **Sung Hoon Kim**[1], **Donald P. McDonnell**[2], **John A. Katzenellenbogen**[1], and **John D. Norris**[2,*]

[1]Department of Chemistry, University of Illinois at Urbana-Champaign, 600 South Mathews Avenue, Urbana, IL 61801

[2]Department of Pharmacology and Cancer Biology, Duke University School of Medicine, Durham, NC 27710

[3]Department of Medicine, Duke University Medical Center, Durham, NC 27710

[4]Duke Cancer Institute, Pharmaceutical Research – PK/PD Core Laboratory, Durham, NC 27710

Abstract

Clinical resistance to the second-generation antiandrogen enzalutamide in castration resistant prostate cancer (CRPC), despite persistent androgen receptor (AR) activity in tumors, highlights the unmet medical need for next generation antagonists. We have identified and characterized tetra-aryl cyclobutanes (CBs) as a new class of competitive AR antagonists that exhibit a unique mechanism of action. These CBs are structurally distinct from current antiandrogens (hydroxyflutamide, bicalutamide, and enzalutamide), and inhibit AR-mediated gene expression, cell proliferation, and tumor growth in several models of CRPC. Conformational profiling revealed that CBs stabilize an AR conformation resembling an unliganded receptor. Using a variety of techniques, it was determined that the AR:CB complex was not recruited to AR-regulated promoters and, like apo AR, remains sequestered in the cytoplasm bound to heat shock proteins. Thus, we have identified third generation AR antagonists whose unique mechanism of action suggests that they may have therapeutic potential in CRPC.

*Corresponding author: jdn001@duke.edu.

[5]Present Address: Department of Chemistry, University of Richmond, 28 Westhampton Way, Richmond, VA 23173

[6]These authors contributed equally to the work.

Author contributions. J.A.P., S.E.W., and A.A.P. contributed equally to this work. A.A.P., J.A.P., S.E.W., J.D.N., D.B.S., S.J.E., H.M.A., C.A.C., S.A.L., I.S., J.G.B., S.H.K., and J.P.S. carried out experiments and analyzed the data. S.E.W., H.M.A., and C.A.C. carried out animal experiments. I.S. designed and carried out PK study. J.A.P., J.D.N., S.E.W., A.A.P., D.P.M., and J.A.K. conceived the project, designed experiments, and wrote the manuscript.

Competing Financial Interests Statement. A patent covering this work has been published (Publication No. WO 2015/048246).

Introduction

Prostate cancer is the most commonly diagnosed cancer among males in the United States, with more than 29,000 men estimated to die from this disease in 2014[1]. The critical driver of prostate tumor progression is the androgen receptor (AR), and when the cancer has progressed past definitive local therapy, therapeutic strategies that target testicular androgen production (LH-RH agonists)[2,3] or competitively inhibit androgen binding to the receptor (AR antagonists) are employed[4]. The suppression of AR function by anti-endocrine therapies is initially effective, but most tumors develop resistance, resulting in a more aggressive cancer known as castration-resistant prostate cancer (CRPC)[5]. CRPC typically exhibits sustained AR signaling through overexpression of the wild type AR[6], upregulation of intratumoral androgen production[7], alternative mRNA splicing resulting in truncated constitutively active AR variants[8–10], or mutations within AR that result in altered receptor pharmacology[11]. Recent sequencing of advanced prostate cancers revealed that 44% of CRPCs had genomic alterations involving AR, with 20% containing an AR point mutation[12]. Mutations in the ligand-binding domain of AR often result in its ability to recognize antiandrogens as agonists. For example, the most common AR mutations, T877A and W741C, enable the first generation AR antagonists, flutamide (OHF) and bicalutamide (Bic), respectively, to function as agonists[13,14]. The second generation antiandrogens enzalutamide (Enz) and ARN-509 were developed to retain antagonist activity in the setting of acquired resistance, where AR mutations and/or overexpression are the most frequently observed[15,16]. Despite the impressive clinical activity of these contemporary antiandrogens, recent studies have revealed the emergence of acquired resistance which has been linked in part to a novel F876L mutation within the ligand-binding domain[17,18]. The discovery of this mutation, which negates the antagonist activity of enzalutamide and enables it to exhibit agonist activity, highlights the need to develop next-generation AR antagonists that are capable of targeting the broadest spectrum of resistance-conferring receptor mutations.

Herein, we describe the discovery and exploration of a tetra-aryl cyclobutane (CB) scaffold as a core building block for the development of next-generation antiandrogens. These tetra-aryl cyclobutane compounds are structurally distinct antiandrogens, act as competitive inhibitors of AR, and obstruct androgen-mediated gene transcription in multiple models of hormone-refractory disease, including those in which mutant ARs (F876L, T877A, and W741C) and wild type AR overexpression are apparent. Importantly, the most potent antagonist of this class does not promote AR nuclear translocation and inhibits the growth of enzalutamide-resistant xenograft tumors.

Results

Cyclobutane (CB)-core ligands are AR antagonists

In an effort to identify inhibitors that overcome enzalutamide resistance, we utilized a CV1 transient transfection system (MMTV-Luciferase reporter gene) expressing AR-F876L to screen an in-house library containing unique small-molecule scaffolds. After eliminating compounds with unsatisfactory toxicity profiles, the tetra-aryl cyclobutane (CB) compound **1** emerged as a promising lead (Supplementary Results, Supplementary Table 1), providing effective inhibition of AR-F876L activity without general cellular toxicity, with an IC_{50} of

1.64 μM. Based upon this finding, an expanded library of cyclobutanes, appended with a variety of substituted arenes, was synthesized using an efficient and, in some cases, regioselective solid-state photodimerization approach[19,20].

As above, the inhibitory activity of the CBs was measured using a CV1 transient transfection system in which AR-F876L was expressed. Substitution of the methoxy group on **1** with larger alkoxy groups **(2-5)**, along with removal of the substitution on the pyrimidine ring (**6**) abolished antagonist activity. However, replacement with a methyl or ethyl group (**7** and **8**, respectively) retained activity. Although the tetra-chloro **9** was not potent, the presence of two-chloro substituents exhibited strong antagonist activity (**10** and **11**). Indeed, at sub-micromolar concentrations, **10** was shown to completely inhibit the activity of AR-F876L. Addition of the methyl group on **12** retained activity. The exchange of the phenyl group with a diphenyl ring (**13**) or a thienyl group (**14** and **17**) was not well tolerated while substitution of the chloro with a methoxy group (**15** and **16**) retained activity. Additionally, thioether, sulfonyl, and amino substitutions were not effective (**18**-**20**).

To assess the therapeutic potential of the CBs, we examined their activity in cellular assays that model different mechanisms by which antiandrogen resistance occurs. To this end, we utilized the CV1 transient transfection assay to evaluate the antagonistic activity of the CBs against wt-AR and two additional mutants, T877A and W741C, associated with treatment failure in patients treated with OHF or Bic, respectively (Supplementary Table 1). The most potent inhibitors of AR-F876L (**1**, **7**, **10**, **11**, **12**, **15**) were equally effective inhibitors of AR-T877A and AR-W741C. Surprisingly, we observed that the potency of the CBs was right shifted when evaluated in the context of wt-AR as opposed to the mutants, with only **10** and **15** having IC_{50} values less than 10 μM. The serendipitous discovery of mutant-selective antagonists suggests that it is possible to develop drugs that spare wt-AR activity. Such drugs may have particular utility in the treatment of late stage disease where cachexia is present and inhibition of wt-AR in muscle (or in the skeleton) is an undesirable activity.

CBs are competitive antagonists of wt and mutant AR forms

Because the structure of the CBs is markedly different from that of earlier generation AR ligands, we set out to define the biochemical basis for their inhibitory activity. Using ^{3}H-R1881 whole-cell competition binding assays, it was determined that all of the compounds tested inhibited agonist binding (Fig. 1a–d), with unlabeled **1**, **10**, and **15** effectively competing with R1881 (synthetic AR agonist) for binding to wt-AR and each mutant AR at concentrations near their predicted IC_{50} values (Supplementary Table 2). **10** demonstrated the highest potency against all AR variants. Consequently, we confirmed that **10** functions as a competitive antagonist of AR by Schild analysis, wherein increasing concentrations of compound did not decrease the maximal R1881-stimulated response of the MMTV luciferase reporter gene but did increase the apparent EC_{50} for R1881 in CV1 cells expressing wt-AR or AR-F876L (Supplementary Fig. 1). In addition, the selectivity of **10** was confirmed by assessing its activity on other nuclear receptors (Supplementary Table 3).

Next we investigated whether **10** could antagonize endogenous AR transcriptional activity in the LNCaP prostate cancer cell line, which expresses AR-T877A. As shown in Fig. 2a, 10

inhibited R1881-dependent expression of *KLK3* (also known as *PSA*), *NKX3-1*, and *FKBP5* mRNA with the same efficacy as enzalutamide. In addition, **10** inhibited androgen-stimulated proliferation of LNCaP cells with similar efficacy to enzalutamide (Fig. 2b). To examine the therapeutic potential of the CBs, we generated two prostate cancer cell lines that model resistance mechanisms apparent in patients with CRPC: LNCaP-AR expressing a high level of AR and LNCaP-F876L expressing the AR mutant that is resistant to enzalutamide. In both cell lines, R1881 induces cell proliferation (Supplementary Fig. 2). We then examined the effectiveness of **1**, **10**, and **15** in inhibiting AR transcriptional activity in these CRPC cell lines.

As shown in Fig. 2c, Bic functioned as a partial agonist in the LNCaP-AR model, inducing substantial AR target gene expression likely accounting for the ineffectiveness of Bic in CRPC[21]. Similar to enzalutamide, the CBs did not promote AR target gene transcription in the LNCaP-AR cells. In the presence of R1881, **10** and **15** reversed androgen-stimulated gene expression, as did enzalutamide (Fig. 2d). However, **1** was less potent in this context likely reflecting its higher IC_{50} for wt-AR. As expected, enzalutamide stimulated rather than inhibited the expression of AR target genes in the LNCaP-F876L cell line. When analyzed in the same manner, the CBs maintained their antagonist activity (Fig. 2e). In addition, when the transcriptional activity of this mutant was analyzed in the presence of R1881, the CBs inhibited gene expression while, as expected, enzalutamide was ineffective (Fig. 2f). Direct quantification of R1881-mediated target gene expression and subsequent **10** inhibition is illustrated for a subset of genes (*KLK3*, *NKX-1*, and *FKBP5*) in Supplementary Fig. 3. In addition to LNCaP cells, we observed that **10** also inhibited androgen-stimulated expression of *KLK3*, *NKX3-1*, and *FKBP5* mRNAs in LAPC4 and VCAP cells, well-established models of prostate cancer in which wt-AR is expressed (Supplementary Fig. 4).

CBs stabilize an apo-like conformation in AR

Previously, we showed that the pharmacological activity of AR ligands is primarily determined by their impact on receptor conformation and consequent coregulator recruitment[22]. This relationship was established using a cell-based conformation-profiling tool that uses coregulator-derived peptides to survey ligand-dependent presentation of protein-protein interaction surfaces as a proxy for receptor structure. This well-validated technology has been used to identify, classify, and accurately predict the biological activity of novel AR agonists and antagonists[23]. Using a variant of this tool optimized to study antagonist pharmacology, we performed a comparative analysis of the impact of benchmark ligands and **1**, **10**, and **15** on AR structure in intact cells (Fig. 3a). Analysis of the interaction data revealed similar cofactor interaction profiles for agonists (R1881, DeHT) and partial agonists (S4)[24]. The antagonists cyproterone acetate (CPA) and RU 486 induce similar conformational changes in receptor structure. As expected, enzalutamide and its related analogs, ARN509 and NC7[16], induce a unique AR conformation but, importantly, are not distinguishable from one another. These compounds show efficacy in certain models of CRPC[15,16]. Interestingly, the AR antagonists that fail to demonstrate efficacy in CRPC (nilutamide, flutamide, and bicalutamide) also cluster together, revealing common features in their mechanism of action. Importantly, the cofactor binding profiles of **1**, **10**, and **15** are most similar to the unliganded receptor (vehicle) and distinct from that of any other AR-

ligand complex, a result which confirms their unique mechanism of action. The similarity of **10**-bound AR to unliganded receptor was confirmed by repeating a selection of cofactors, RN28S1 and HLA-B, in the presence of R1881 at the concentration of **10** utilized in the profiling experiment (Supplementary Fig. 5).

CBs block recruitment of AR to target gene promoters

To further discern the mechanisms underlying the unique activity of the CBs, we performed chromatin immunoprecipitation (ChIP) assays in both LNCaP-AR (Fig. 3b) and LNCaP-F876L (Fig. 3c) cells and compared the ability of selected compounds to recruit AR to the regulatory regions of the androgen-regulated *KLK3* and *NKX3-1* genes. In the LNCaP-AR cells, Bic and R1881 facilitated AR recruitment to DNA, whereas enzalutamide and **10** were without effect (Fig. 3b). In the LNCaP-F876L model, however, enzalutamide promoted the binding of AR to DNA while **10** remained effective as an inhibitor of AR-DNA binding; **10** inhibited AR recruitment more effectively than Bic (Fig. 3c). Thus, the unique changes in AR conformation noted above translate into a useful pharmacological activity.

CBs prevent androgen-mediated AR nuclear translocation

The observation that **10**-bound AR adopts an apo-like conformation and disrupts AR-DNA interactions suggested that the **10**-receptor complex might be sequestered in the cytoplasm. Thus, we used high content imaging (Cellomics ArrayScan) to perform unbiased quantification of AR subcellular distribution when complexed with **10**, enzalutamide, and/or R1881. As expected, we observed an increase in AR nuclear-to-cytoplasmic (N/C) ratio upon addition of the agonist R1881 in VCaP prostate cancer cells as well as in HEK293 cells expressing wt-AR (Fig. 4a). Enzalutamide treatment, in the absence and presence of R1881, was also found to increase the AR N/C ratio; this observation was somewhat surprising given that previous studies have shown that enzalutamide blocks nuclear translocation of the receptor[16]. Conversely, treatment with **10** did not promote AR nuclear localization, even upon cotreatment of cells with R1881 (Fig. 4a). Representative images from the VCaP analysis are shown in Fig. 4b. To further validate the ability of **10** to block androgen-mediated nuclear AR translocation, we performed subcellular fractionation experiments in HEK293 cells expressing wt-AR. Consistent with the imaging experiments, treatment of cells with R1881 resulted in the movement of AR from the cytoplasmic to nuclear fraction. Cotreatment of cells with **10** and R1881 demonstrated that **10**, unlike enzalutamide, completely abrogated androgen-mediated accumulation of nuclear AR (Fig. 4c). When assessed by high content imaging, treatment of HEK293 cells expressing AR-F876L with **10** also resulted in inhibition of androgen-mediated nuclear accumulation (Supplementary Fig. 6). As expected, enzalutamide treatment resulted in a robust increase in AR N/C ratio in this model. Despite differential localization of AR, **10** does not promote AR degradation (Supplementary Fig. 7a–b).

It has been established that unliganded AR is located in the cytoplasm as part of a large multiprotein complex including heat shock proteins HSP90 and HSP70[25,26]. Upon androgen binding, a conformational change in the receptor results in loss of HSP90 binding, exposes a nuclear localization signal (NLS) within the receptor, and facilitates nuclear import. Given that the AR- **10** complex resembles unliganded receptor and is thus retained in the

cytoplasm, we set out to determine the impact of **10** binding on the interaction of AR with HSP90. We performed co-immunoprecipitation experiments with androgen-, **10**-, or enzalutamide-bound AR and assessed the ability of the different complexes to interact with HSP90. R1881- and enzalutamide-bound AR were found to displace HSP90 from the receptor while **10**-bound receptor maintained its interaction with HSP90, similar to apo-AR (Fig. 4d). Taken together, these data highlight a unique mechanism of action for the antagonist activity of **10** whereby as a result of its inability to displace HSP90 from AR, the receptor remains in the cytoplasm.

10 inhibits proliferation in cellular models of CRPC

To explore the impact of CBs on prostate cancer cell growth, we assessed the effects of **10** on the growth of AR-overexpressing prostate cancer cells (LNCaP-AR) and in cells that are resistant to enzalutamide (LNCaP-F876L). As expected, Bic promoted cellular proliferation in AR overexpressing cells; however, enzalutamide and **10** were without effect (Fig. 5a). Similarly, in the enzalutamide-resistant cells, enzalutamide, but not **10** or Bic, promoted cellulars proliferation (Fig. 5b). Furthermore, **10** was able to inhibit R1881-mediated proliferation of AR-expressing VCaP cells, but not the growth of AR-negative cell lines PC3 or DU145 (Supplementary Fig. 8a–c). These results highlight an important selective phenotypic consequence of the unique differences exhibited by **10** in the studies outlined above.

10 suppresses tumor growth in animal models of CRPC

Given the effect of **10** on the growth of CRPC cells, we proceeded to evaluate its activity in relevant xenograft models of prostate cancer. The initial studies were performed in intact male mice bearing LNCaP xenografts where the activity of enzalutamide (15 mpk) or escalating doses of **10** (5 to 100 mpk) were evaluated. Of note, 15 mg/kg enzalutamide, experimentally determined to be the MTD for this antiandrogen in NSG mice when administered i.p., was sufficient to inhibit AR activation in both tumor and endogenous tissues. In this study it was noted that administration of **10** (50 or 100 mpk) significantly inhibited androgen-responsive LNCaP prostate cancer tumor growth (Supplementary Fig. 9). To further evaluate the therapeutic potential of **10**, we generated a mouse model in which enzalutamide-resistant AR-F876L cells were propagated as xenografts. For this study, castrated male mice bearing AR-F876L xenografts were treated with vehicle, enzalutamide (15 mpk), or escalating doses of **10** (30 to 100 mpk). As expected, these tumors grew in the absence of androgens (vehicle), and enzalutamide treatment failed to inhibit tumor growth[18,21]. Notably, treatment with **10** (50 or 100 mpk) completely suppressed ($p < 0.0001$) tumor growth for the entire 28-day treatment period (Fig. 5c), with the higher dose showing a trend towards tumor regression. Although the dose of **10** was higher than what was used for enzalutamide, we did not observe any changes in the behavior or health of the animals with even the highest dose of **10** treatment. Analysis of **10** drug levels (Supplementary Fig. 10a) in plasma 24 hours after final treatment showed that the 50 (0.9±0.44 μM) and 100 mg/kg (1.25±0.74 μM) doses were sufficient to inhibit AR F876L activity based on the **10** transcriptional IC_{50} value reported in Supplementary Table 1. Furthermore, a single dose pharmacokinetic study (100 mg/kg) performed in F876L tumor-bearing mice revealed that

drug levels of **10** in the tumor ranged from 31.3 μM (1.5 hr post treatment) to 1.1 μM (24 hr post treatment), concentrations that are not toxic to prostate cancer cells *in vitro* (Supplementary Fig. 10b). In addition, the on-target activity of **10** was confirmed when the growth of (androgen-independent) 22Rv1 xenograft tumors was not influenced by treatment with **10** (Supplementary Fig. 11).

Discussion

While the majority of prostate cancers develop resistance to FDA-approved inhibitors of AR signaling, abundant clinical evidence suggests that in most CRPC, AR remains a viable target and is engaged in the regulation of processes of pathological importance. Thus, there is a significant unmet medical need for novel modulators of AR function for use in the treatment of hormone-refractory prostate cancer. The mechanisms underlying resistance to existing endocrine therapies include activation of secondary signaling cascades that increase AR activity, AR overexpression[6], AR mutation[4], and increased expression of constitutively active AR splice variants[8–10]. It is significant, therefore, that we have identified a class of compounds that act as competitive AR antagonists with a novel cyclobutane structure and unique activity profile. While these compounds are not effective against constitutively active AR variants that lack the ligand binding domain, **10** was found to inhibit full-length endogenous AR-regulated gene expression, slow PC cellular proliferation, and halt prostate tumor growth. More specifically, these CBs are of particular interest because they effectively inhibit AR in the context of receptor-overexpression and inhibit the activity of AR mutants that arise during enzalutamide (F876L), OHF (T877A), and Bic (W741C) treatment. Previously described discovery campaigns in this area have focused on the development of compounds that inhibit the T877A and W741C mutant receptors[27–29] or on derivatives of enzalutamide that retain activity against the F876L mutant[21,30]. Our CBs, however, form a particularly promising class of antagonists that are structurally dissimilar to earlier generation AR antagonists and exhibit pan-mutant inhibitory activity.

Interestingly, some of the most potent CBs we have studied exhibit a 10 to 30-fold increased affinity and potency for the F876L AR over wild type receptor, suggesting the possibility for selective targeting of mutant AR signaling associated with previously treated hormone-refractory prostate cancer. Mutant-selective AR inhibitors may provide effective therapy for hormone-refractory prostate cancer, while avoiding some of the negative side effects associated with androgen deprivation in other tissues (muscle and bone density loss, decreased libido, etc.). This approach has proven valuable in targeting the mutant form of BRAF, and in 2011, the FDA approved vemurafenib (PLX4032/RG7204, Plexxikon/Roche) for the treatment of metastatic melanoma bearing the BRAF V600E mutation[31–33]. It is anticipated that mutant-selective CBs, such as those described here, could provide a valuable basis for the development of therapeutics to treat advanced prostate cancer in a more effective and selective fashion.

The signature structural element of our AR antagonists is their cyclobutane core. While not unprecedented in medicinal compounds, cyclobutane-core structural components are relatively rare in both natural products and synthetic bioactive compounds. Most naturally occurring molecules in this class arise from sunlight-initiated [2+2] cycloaddition reactions

of stilbene or cinnamic acid-like precursors, leading to symmetric or quasi-symmetric tetra-substituted cyclobutane dimers[34–39]. Coincidentally, examples of novel, synthetically-derived bioactive cyclobutane-core compounds have also been isolated from the accidental photodimerization of drug candidates containing photo-active π-systems[40,41]. Despite their rarity, substituted cyclobutanes are intriguing as scaffolds for molecular probes and drug candidates due to their inherent three-dimensionality. In fact, molecules with a cyclobutane core have recently shown promise as agonists of glucagon-like peptide-1 (GLP-1) receptor *in vitro* and *in vivo*[41,42]. In addition, the conformational rigidity of the cyclobutane has been utilized in the development of peptidomimetic inhibitors of metallocarboxypeptidases[43]. Our work expands the utility of cyclobutane-containing molecules as novel AR inhibitors in models of CRPC. In particular, the capacity of **10** to inhibit agonist induced transcription and proliferation in LNCaP and VCaP cells, and the ability to inhibit AR in multiple models of CRPC, suggests that optimized cyclobutanes of this class may become practical therapeutics for hormone-refractory prostate cancer. The striking inhibition of both wt and F876L AR-containing tumors with **10** in murine models demonstrates that these compounds retain their activity *in vivo*, further supporting their position as viable medicinal candidates.

The structural uniqueness of the CBs translates to differences in their mechanism of action.. Similar to enzalutamide, the CBs reduce the recruitment of AR to gene-regulatory chromatin binding sites. However, in contrast to enzalutamide and other antiandrogens, the unique structure of the CBs stabilise a conformation in AR that is most similar to the apo-receptor. Hence, by binding to AR with minimal disruption in receptor structure, the CBs foster an AR:CB complex that remains bound to HSP90 in the cytoplasm, thereby inhibiting nuclear localization and recruitment to chromatin. This novel mechanism helps explain their notable anti-tumor activity in animal models of CRPC and suggests that **10** has the potential to be exploited as an AR antagonist with a distinctive mechanistic profile.

Online Methods

Reagents

R1881 and ^{3}H-R1881 were purchased from Perkin Elmer. Enzalutamide, bicalutamide, and flutamide were purchased from Cayman Chemical Company (> 98% purity). Antibodies for AR (N-20, SC-27316, 1:10,000; 441, SC-7305, 1:10,000), α-tubulin (E-19, SC-27316, 1:10,000), Topoisomerase 1 (C-21, SC-32736, 1:5,000), and HSP90 (F-8, SC-13119, 1:1,000) were purchased from Santa Cruz Biotechnology. Antibody for β-actin (AC-15, A5441, 1:10,000) was purchased from Sigma. LNCaP, PC3, and 22rv1 cells were maintained in RPMI supplemented with 8% fetal bovine serum (FBS). VCAP, HEK293, and DU145 cells were maintained in DMEM (8% FBS) and LAPC4 cells were maintained in IMDM (15% FBS). All cell lines were obtained from ATCC which uses short tandem repeat (STR) DNA profiles for authentication. None of the cell lines used for these studies are listed in the database of commonly misidentified cell lines maintained by ICLAC. All cell lines tested negative for mycoplasma. Stable LNCaP cell lines expressing wt-AR (LNCaP-AR), F876L mutation (LNCaP-F876L), or empty vector control (LNCaP-XIP) were generated using pQC-XIP retrovirus vector (Promega).

Prostate Cancer Cell Proliferation Assay

Cells were plated in 96-well plates (10k cells/well) and treated with hormone for 7 days. Cellular proliferation was quantified by measuring DNA content using Hoechst dye[1].

RNA Isolation and Real-Time PCR

LNCaP-XIP, LNCaP-AR, or LNCaP-F876L cells were seeded in 12-well plates in RPMI 1640 (8% charcoal-stripped fetal calf serum (CFS)). After 48 hrs, cells were treated with ligand (18 hrs) and total RNA was isolated using the Aurum Total RNA Mini Kit (Bio-Rad). AR target gene transcription was assessed by realtime PCR as described previously[2]. Data are normalized to the GAPDH housekeeping gene. For heatmaps, the data were first normalized to the vehicle control. Data were then standardized using the following equation, $Z= X – \mu/\sigma$, where X is the normalized signal (zero centered), μ is the average signal for all conditions within a gene, and σ is the standard deviation (SD) for all conditions within a gene. The data were then clustered by the Ward hierarchical clustering method using JMP (SAS).

Chromatin Immunoprecipitation Assay

LNCaP-AR and LNCaP-F876L cells were plated in 150 mm dishes in RPMI 1640 (8% CFS). Following 48 hr incubation, cells were treated with ligand for 4 hr. 1% formaldehyde was added (10 min) and quenched with 250 mM glycine (5 min). Cells were washed twice with PBS, pelleted, lysed in RIPA buffer (50 mM Tris [pH 7.5], 0.15 M NaCl, 1% NP-40, 0.5% Na-deoxycholate, 0.05% SDS, 1 mM EDTA), sonicated, and then processed for chromatin immunoprecipitation using either anti-AR (N-20) or IgG antibodies (Santa Cruz), as previously described[44].

High Content Imaging

Cells were fixed with 4% paraformaldehyde in PBS, permeabilized with 0.1% Triton X-100, and stained for AR (1:400, N-20, Santa Cruz) and counterstained for DNA (DAPI, Sigma) and F-actin (rhodamine Phalloidin, Thermo Fisher Scientific). Stained cells were imaged and analyzed with a Cellomics ArrayScan VTI HCS system. 20 fields per well of a 24-well plate were imaged at 20× magnification and analyzed using the Compartmental Analysis Bioapplication. First, images were collected by autofocusing on nuclear staining in channel 1. Cells were then identified in channel 1, indicated as valid object count (VOC). Nuclear:Cytoplasmic ratio of AR staining was determined by measuring channel 2 signal within the nuclear mask identified in channel 1 versus the cytoplasmic area, which was approximated by extending 2 pixels outside of the nuclear mask. Experiments were performed in triplicate and repeated five times.

AR Conformation Profiling Assay

HepG2 cells were maintained in Basal Medium Eagles (10% FBS). For mammalian two-hybrid based AR cofactor profiling assays, cells were transfected with VP16-AR, 5XGalLuc3, Gal4-interactor, and Renilla-Luciferase. Cells were induced with ligand (48 hr) and then dual luciferase assays were performed. Renilla luciferase served as control for cellular toxicity and transfection efficiency. The data was standardized to avoid bias due to

signal strength and clustered with the Ward hierarchical clustering method using JMP (SAS)[22]. The hierarchical cluster dendrogram was ordered by the first principal component.

Reporter Gene Assay

CV1 cells were seeded into 96-well cell culture plates and transfected with Lipofectin (Invitrogen) according to the manufacturer's protocol. For AR transcriptional assays, the DNA mixture consisted of pcDNA-AR (wt or mutant), MMTV-Luc (reporter gene), and Renilla-Luc (for assessing transfection efficiency and toxicity). Following overnight incubation, cells were induced with hormone for 24 hrs. Cells were lysed and luciferase activity was quantified using Dual Luciferase Reagent (DLR).

Whole Cell Competition Binding Assay

HEK293 cells were transfected with vectors expressing wt-AR or AR mutants using FuGene6 (Promega) and 100,000 cells were plated in a 24-well plate (DMEM, 8% CFS) coated with 0.2% gelatin. Following overnight incubation, cells were treated with ligand in the presence of 0.1 nM ^{3}H-R1881. To determine background levels of radioactivity, control wells were treated with 500X cold R1881 (50 nM). After 2 hr incubation, cells were lysed using 200 μl lysis buffer (2% SDS, 10% Glycerol, 10 mM Tris-HCl [pH 6.8]); then volumes were increased to 500 μl using 10 mM Tris-HCl (pH 8.0). 300 μl of the lysates were added to 3 mL of Cytoscint (MP Biomedicals) and analyzed by scintillation counting (Beckman LS 6000SC). Lysate protein levels were quantified using the Pierce BCA Protein Assay Kit (Thermo Scientific) per the manufacturer's instructions.

In-Cell Western Assay

LNCaP cells were plated in 96-well clear bottom black plates (20K cells/well) in RPMI supplemented with 8% CFS. Following 48 hr incubation, cells were treated with hormone for 18 hrs. Cells were fixed with formaldehyde (3.7%) and permeabilized using PBS (0.1% TRITON X-100). Cells were incubated with anti-AR antibody (N20, 1:2000), washed with PBS (0.1% Tween), and stained with 2nd antibody (Biotium CF770 goat anti-rabbit, 1:2000). AR protein expression was assessed using the LI-COR Odyssey imaging system. DRAQ5 (DNA stain, 1:10,000, Thermo Scientific) was used to normalize AR protein expression.

Western Analysis

LNCaP cells were plated in RPMI supplemented with 8% CFS. Following 48 hr incubation, cells were treated with hormone for 18 hr. Cells were lysed (50 mM Tris, pH 7.5, 150 mM NaCl, 1% NP-40, 0.5% Na-deoxycholate, 0.05% SDS, 5 mM EDTA, 50 mM NaF, 15 mM Na-pyrophosphate, 10 mM β-glycerophosphate, 2 mM Na-orthovanadate, 1X protease inhibitor cocktail) and cleared whole cell extracts were analyzed by Bradford assay. 50 μg of protein per sample were resolved by SDS-PAGE (8%), transferred to nitrocellulose membrane, and analyzed by western blot using antibodies to AR (N-20, Santa Cruz) and β-actin (Sigma) per manufacturer's instructions.

Cellular Fractionation Assay

HEK293 cells were transfected with wt-AR expression vector using FuGene6. Following overnight incubation, cells were treated for 4 hr with ligand in the absence and presence of R1881 (0.1 nM). Nuclear and cytoplasmic fractions were obtained using NE-PER reagent from Thermo Scientific (78835) according to manufacturers instructions. Proteins were subjected to SDS/PAGE and western blotting using AR (N-20, Santa Cruz), α-tubulin (E-19, Santa Cruz), and topoisomerase 1 (C-21, Santa Cruz) antibodies.

Co-Immunoprecipitation Assay

HEK293 cells were transfected with wt-AR expression vector using FuGene6. Following overnight incubation, cells were treated for 4 hr with ligand in the absence and presence of R1881 (0.1nM). Cells were lysed in immunoprecipitation (IP) buffer (20 mM Tris HCl pH 7.5, 50 mM NaCl, 20 mM Na_2MoO_4, 0.5% Nonidet P-40 (NP-40), 1 mM EDTA, 1 mM EGTA (pH 8.0), 2 mM DTT, plus protease inhibitors) and incubated for 15 min at 4C. Lysates were pre-cleared with normal rabbit IgG (Santa Cruz) and Protein A/G Plus – Agarose beads (Santa Cruz). Pre-cleared lysates (500 μg total protein) were incubated with 10μg anti-AR antibody (N-20) or normal rabbit IgG overnight at 4C. 50 μl Protein A/G Plus – Agarose beads were added for 4 hr at 4C. Beads were washed 3X with IP buffer and immunoprecipitated proteins were subjected to SDS/PAGE and western blotting using AR 441 (gift from Dr. Dean Edwards, University of Colorado Heath Sciences Center) and HSP90 (F-8, Santa Cruz) antibodies.

Animal Studies

All procedures were approved by the Duke University Institutional Animal Care and Use Committee. *LNCaP-F876L xenograft study:* Male NSG (NOD.Cg-Prkdc^{scid} Il2rg^{tm1Wjl}/SzJ) mice were castrated at 6 weeks of age, 10 days prior to injection of 3×10^6 LNCaP-AR F876L cells sc into the flank. Tumor growth was measured 3x weekly by caliper (tumor volume = (A^2 x B)/2, where A < B). When tumor volume reached ~0.1 cm^3, mice were randomized (n = 12–14) to 28 days of daily i.p. injection with vehicle (10% DMSO, 30% PEG400, 60% corn oil), enz (15 mg/kg) or **10** (30–100 mg/kg). *PK time course:* 6-week old male NSG (NOD.Cg-Prkdc^{scid} Il2rg^{tm1Wjl}/SzJ) mice were castrated 10 days prior to sc injection of 3×10^6 LNCaP-AR-F876L cells (1:1 with matrigel) into the flank. Tumor growth was measured 3x weekly by caliper (tumor volume = (A^2 x B)/2, where A < B). When tumor volume reached ~1 cm^3, 100 mg/kg **10** (vehicle formulation: DMSO:PEG 400:corn oil, 1:3:6) was administered by i.p. injection. Animals (n = 3 per time point) were euthanized 10 min, 30 min, 1.5 hr, 3 hr, 8 hr, and 24 hr after injection, and blood and tissues were retained for analysis. *LNCaP xenograft assay:* 2.5 × 106 LNCaP cells (1:1 with matrigel) were injected sc into the flank of 6-week old male NSG (NOD.Cg-Prkdc^{scid} Il2rg^{tm1Wjl}/SzJ) mice. Tumor growth was measured 3x weekly by caliper (tumor volume = (A^2 x B)/2, where A < B). When tumor volume reached ~0.1 cm^3, mice were randomized (n = 9–15) to 28 days of daily i.p. injection with vehicle (as above), Enz (15 mg/kg) or **10** (5–100 mg/kg). 8 additional mice were castrated and received daily vehicle treatment. *22RV1 xenograft assay:* 6 week old male NU/NU mice were castrated 10 days prior to injection of 1×10^6 22RV1 cells sc and tumor measurement as above. When tumor volume reached 0.11–

0.18 cm^3, mice were randomized to 14 days of daily i.p. injection with vehicle (n = 4) or **10** (100 mg/kg, n = 5) formulated as above. All Statistical analyses were performed using GraphPad Prism 6 and are described in the Statistics section below.

PK sample collection and processing—Blood was collected into heparinized polypropylene (PP) 1.5-mL tubes (10 μL of 1000 U/mL heparin for up to 0.5 mL blood) and plasma separated at 1300 g for 10 min at RT. All specimens were stored at −80 °C until the day of analysis. Tissue was homogenized with 2 parts water (w/v), either by rotary homogenizer (PTFE rotor/glass tube; liver) or by cryo-crushing under liquid nitrogen (stainless in-house made tool; tumor and muscle). Into 200-μL PP tube, 20 μL of either blood, plasma, or tissue homogenate and 40 μL of methanol/acetonitrile (1/1, v/v, containing 2.5 μg/mL **10** deuterium labeled internal std.) was added and vigorously agitated in FastPrep vortexer (Thermo-Savant) at speed 4 for 20 sec. After centrifugation at 13,600 g for 5 min at RT, 5 μL of supernatant was mixed with 195 μL of mobile phase A/acetonitrile (1/1, v/v; see below) and 5 μL injected into LC/MS/MS system.

Liquid chromatography tandem-mass spectrometry (LC/MS/MS)—The analysis was performed on Shimadzu 20A series LC system coupled with Applied Biosciences/ SCIEX API 4000 QTrap MS/MS spectrometer. Column: Phenomenex, C18 4×3 mm guard cartridge (P/N AJ0-4287) and Agilent ZORBAX Eclipse Plus, C18 4.6×50 mm 1.8 μm particle size (P/N 959941-902) analytical column at 35 °C. Mobile phase solvents (all MS-grade): A - 0.1% formic acid in water, 2% acetonitrile; B – acetonitrile. Elution gradient at 1 mL/min: 0–1.5 min 30–95% B, 1.5–2.5 min 95% B, 2.5–2.7 min 95–30% B. Run time: 7 min. MRM transitions for **10** and labeled **10** (m/z): 433.0/217.0 and 443.1/222, respectively. Positive-ion mode. DP: 66 V, EP: 10 V, ion-spray voltage: 5500 V, curtain gas: 30, ion-source gas 1: 30, ion-source gas 2: 25. Lower limits of quantification (LLOQ) for plasma, blood, liver, muscle, and tumor were: 0.08, 0.16, 0.16, 0.08 and 0.08 μg/mL, respectively. Calibration curve samples (n=6) were prepared by adding increasing amounts of **10** to control matrix (plasma, blood, or tissue homogenate) obtained from non-treated animals.

Statistical Analyses

For *in vitro* studies, s.d. and s.e.m. are reported in figure legends for technical and biological replicates. Nuclear/cytoplasmic AR ratios as detected by Cellomics analysis (Figure 4) were subjected to one-way ANOVA comparison followed by Bonferroni multiple comparisons test. Statistically similar ($p < 0.05$) groups are indicated by letters a–d.

For LNCaP-AR-F876L xenograft study, using the sample size and power function in JMP statistical software (SAS Institute, Inc), it was estimated that a group size of N = 13 per treatment arm would be required to reliably detect a statistically relevant ($p<0.05$) 25% change with 80% confidence, given the anticipated 15% variability for the tumor models utilized in these studies ($\alpha = 0.05$, st. dev. = 0.15, confidence of 0.8, s/delta of 0.25). This estimate is based on one way ANOVA followed by the Student Newman Keul's test. This group size is in accordance with current literature in the field. Animals were randomized to treatment when tumor size measured 0.12–0.17 cm^3 volume. Animals were allocated to treatment such that the initial tumor volume average per group was 0.15 +/− 0.015 cm^3

volume. Group size for each treatment arm was as follows: Vehicle 14, Enzalutamide 14, **10** 30 mg/kg 14, **10** 50 mg/kg 13, **10** 100 mg/kg 13. One animal (**10** 100 mg/kg) died prior to the conclusion of the study and was therefore excluded from the presented data and from post-study statistical analyses. All other animals were included. The investigator and personnel were not blinded during this study. Average tumor volume and s.e.m. for each group over 28 days of dosing are presented in Figure 5c. These data were subjected to exponential growth curve analysis constrained to share an initial value, and to two-way ANOVA analysis followed by Bonferroni multiple comparison test. **10** 50 mg/kg and **10** 100 mg/kg were found to significantly differ from the vehicle treated control ($p<0.0001$) on days 14–28 of treatment. All other treatments were statistically similar to the vehicle control throughout the study. Groups showed equivalent variance (10–15% with normal distribution) throughout all time points, justifying the statistical analyses that were selected.

For LNCaP xenograft study, using the sample size and power function in JMP statistical software (SAS Institute, Inc) it was estimated that an intended group size of 14 per treatment arm would be required to reliably detect with 80% confidence a statistically relevant ($p<0.05$) change of 30% given the anticipated 15% variability for the tumor models utilized in these studies ($\alpha=.05$, st dev = 0.15, confidence of 0.8, s/delta of 0.3). For those groups in which 35% or greater change was anticipated (i.e. castrate), fewer animals were anticipated to be required, and the groups were weighted accordingly. These estimates were based on one way ANOVA followed by the Student Newman Keul's test. This group size is in accordance with current literature in the field. Animals were randomized to treatment when tumor size measured 0.1–0.2 cm^3 volume. Animals were allocated to treatment such that the initial tumor volume average per group was 0.15 +/− 0.02 cm^3 volume. Group size for each treatment arm was as follows: Vehicle 15, Enzalutamide 15, **10** 5 mg/kg 13, **10** 15 mg/kg 13, **10** 50 mg/kg 10, **10** 100 mg/kg 10, castrate 8. One animal (**10** 50 mg/kg) died prior to the conclusion of the study and was therefore excluded from the presented data and from post-study statistical analyses. All other animals were included. The investigator and personnel were not blinded during these studies. Survival curve analysis was used to detect significant difference in days to reach 0.5 cm^3 volume, an endpoint arbitrarily selected prior to initiating the study. All treatments resulted in a significant delay in time to endpoint as compared to the vehicle control, as determined by Logrank (Mantel-Cox) test.

For the 22RV1 xenograft study, JMP analysis ($\alpha = 0.05$, st. dev. = 0.10, confidence of 0.8, s/delta of 0.4) advised the use of 5 animals per treatment arm. Group size for each treatment arm contained 5 animals. One vehicle treated animal died prior to the conclusion of the study and was excluded from the statistical analyses. Average tumor volume and S.E.M. for each group over 14 days of dosing are presented in Supplementary Fig. 11. These data were subjected to exponential growth curve analysis constrained to share an initial value, and to two-way ANOVA analysis followed by Bonferroni multiple comparison test. No significant difference was detected between these treatments.

Supplementary Material

Refer to Web version on PubMed Central for supplementary material.

Acknowledgments

This work was supported by grants from the CDMRP (Synergistic Idea Development Award W81XWH-10-1-0179 to DPM and JAK), the NIH (PHS5R01DK015556 to JAK), and the DOD (W81XWH-13-1-0196 to JDN). JAP was supported by an NIH Training grant (T32ES007326). AAP was supported by NIH NRSA (1 F30 DK083899). We would like to thank Jillian R. Gunther, Kathy E. Carlson, and Teresa A. Martin for their early contributions to the project. We are thankful to Ping Fan, MS, for performing the LC/MS/MS assays within the PK/PD Core Laboratory. I.S. is grateful for the support of the Pharmaceutical Research Shared resource - PK/PD Core laboratory by NIH/NCI Core Grant, 5-P30-CA14236-29.

References

1. Siegel R, Ma J, Zou Z, Jemal A. Cancer statistics, 2014. CA Cancer J Clin. 2014; 64:9–29. [PubMed: 24399786]
2. Rick FG, Schally AV. Bench-to-bedside development of agonists and antagonists of luteinizing hormone-releasing hormone for treatment of advanced prostate cancer. Urol Oncol. 2015; 33:270–274. [PubMed: 25512159]
3. Rick FG, Block NL, Schally AV. An update on the use of degarelix in the treatment of advanced hormone-dependent prostate cancer. Onco Targets Ther. 2013; 6:391–402. [PubMed: 23620672]
4. Chen Y, Sawyers CL, Scher HI. Targeting the androgen receptor pathway in prostate cancer. Curr Opin Pharmacol. 2008; 8:440–8. [PubMed: 18674639]
5. Klein KA, et al. Progression of metastatic human prostate cancer to androgen independence in immunodeficient SCID mice. Nat Med. 1997; 3:402–8. [PubMed: 9095173]
6. Edwards J, Krishna NS, Grigor KM, Bartlett JM. Androgen receptor gene amplification and protein expression in hormone refractory prostate cancer. Br J Cancer. 2003; 89:552–6. [PubMed: 12888829]
7. Locke JA, et al. Androgen levels increase by intratumoral de novo steroidogenesis during progression of castration-resistant prostate cancer. Cancer Res. 2008; 68:6407–15. [PubMed: 18676866]
8. Dehm SM, Tindall DJ. Alternatively spliced androgen receptor variants. Endocr Relat Cancer. 2011; 18:R183–96. [PubMed: 21778211]
9. Li Y, et al. AR intragenic deletions linked to androgen receptor splice variant expression and activity in models of prostate cancer progression. Oncogene. 2012; 31:4759–67. [PubMed: 22266865]
10. Nakazawa M, Antonarakis ES, Luo J. Androgen receptor splice variants in the era of enzalutamide and abiraterone. Horm Cancer. 2014; 5:265–73. [PubMed: 25048254]
11. Chen CD, et al. Molecular determinants of resistance to antiandrogen therapy. Nat Med. 2004; 10:33–9. [PubMed: 14702632]
12. Beltran H, et al. Targeted next-generation sequencing of advanced prostate cancer identifies potential therapeutic targets and disease heterogeneity. Eur Urol. 2013; 63:920–6. [PubMed: 22981675]
13. Hara T, et al. Novel mutations of androgen receptor: a possible mechanism of bicalutamide withdrawal syndrome. Cancer Res. 2003; 63:149–53. [PubMed: 12517791]
14. Veldscholte J, et al. A mutation in the ligand binding domain of the androgen receptor of human LNCaP cells affects steroid binding characteristics and response to anti-androgens. Biochem Biophys Res Commun. 1990; 173:534–40. [PubMed: 2260966]
15. Clegg NJ, et al. ARN-509: a novel antiandrogen for prostate cancer treatment. Cancer Res. 2012; 72:1494–503. [PubMed: 22266222]
16. Tran C, et al. Development of a Second-Generation Antiandrogen for Treatment of Advanced Prostate Cancer. Science. 2009; 324:787–790. [PubMed: 19359544]
17. Joseph JD, et al. A clinically relevant androgen receptor mutation confers resistance to second-generation antiandrogens enzalutamide and ARN-509. Cancer Discov. 2013; 3:1020–9. [PubMed: 23779130]
18. Korpal M, et al. An F876L mutation in androgen receptor confers genetic and phenotypic resistance to MDV3100 (enzalutamide). Cancer Discov. 2013; 3:1030–43. [PubMed: 23842682]

19. Parent AA, Gunther JR, Katzenellenbogen JA. Blocking Estrogen Signaling After the Hormone: Pyrimidine-Core Inhibitors of Estrogen Receptor-Coactivator Binding. J Med Chem. 2008; 51:6512–6530. [PubMed: 18785725]
20. Parent AA, Ess DH, Katzenellenbogen JA. pi-pi interaction energies as determinants of the photodimerization of mono-, di-, and triazastilbenes. J Org Chem. 2014; 79:5448–62. [PubMed: 24837276]
21. Balbas MD, et al. Overcoming mutation-based resistance to antiandrogens with rational drug design. Elife. 2013; 2:e00499. [PubMed: 23580326]
22. Norris JD, et al. Differential Presentation of Protein Interaction Surfaces on the Androgen Receptor Defines the Pharmacological Actions of Bound Ligands. Chem Biol (Cambridge, MA, US). 2009; 16:452–460.
23. Joseph JD, et al. Inhibition of prostate cancer cell growth by second-site androgen receptor antagonists. Proc Natl Acad Sci U S A. 2009; 106:12178–12183. S12178/1–S12178/13. [PubMed: 19574450]
24. Yin D, et al. Pharmacodynamics of selective androgen receptor modulators. J Pharmacol Exp Ther. 2003; 304:1334–40. [PubMed: 12604714]
25. Gillis JL, et al. Constitutively-active androgen receptor variants function independently of the HSP90 chaperone but do not confer resistance to HSP90 inhibitors. Oncotarget. 2013; 4:691–704. [PubMed: 23674566]
26. Ni L, et al. FKBP51 promotes assembly of the Hsp90 chaperone complex and regulates androgen receptor signaling in prostate cancer cells. Mol Cell Biol. 2010; 30:1243–53. [PubMed: 20048054]
27. Oh S, Nam HJ, Park J, Beak SH, Park SB. Development of a benzopyran-containing androgen receptor antagonist to treat antiandrogen-resistant prostate cancer. Chem Med Chem. 2010; 5:529–33. [PubMed: 20135667]
28. Wakabayashi K, Imai K, Miyachi H, Hashimoto Y, Tanatani A. 4-(Anilino)pyrrole-2-carboxamides: Novel non-steroidal/non-anilide type androgen antagonists effective upon human prostate tumor LNCaP cells with mutated nuclear androgen receptor. Bioorg Med Chem. 2008; 16:6799–812. [PubMed: 18571420]
29. Yamamoto S, et al. Design, synthesis, and biological evaluation of 3-aryl-3-hydroxy-1-phenylpyrrolidine derivatives as novel androgen receptor antagonists. Bioorg Med Chem. 2013; 21:70–83. [PubMed: 23199477]
30. Kuruma H, et al. A novel antiandrogen, Compound 30, suppresses castration-resistant and MDV3100-resistant prostate cancer growth in vitro and in vivo. Mol Cancer Ther. 2013; 12:567–76. [PubMed: 23493310]
31. Bollag G, et al. Clinical efficacy of a RAF inhibitor needs broad target blockade in BRAF-mutant melanoma. Nature. 2010; 467:596–9. [PubMed: 20823850]
32. Flaherty K, et al. Phase I study of PLX4032: Proof of concept for V600E BRAF mutation as a therapeutic target in human cancer. Journal of Clinical Oncology. 2009; 27
33. Flaherty KT, et al. Inhibition of mutated, activated BRAF in metastatic melanoma. N Engl J Med. 2010; 363:809–19. [PubMed: 20818844]
34. Davis RA, et al. Endiandrin A, a Potent Glucocorticoid Receptor Binder Isolated from the Australian Plant Endiandra anthropophagorum. J Nat Prod. 2007; 70:1118–1121. [PubMed: 17583952]
35. Dembitsky VM. Bioactive cyclobutane-containing alkaloids. J Nat Med. 2008; 62:1–33. [PubMed: 18404338]
36. Lu Y, Foo LY. Rosmarinic acid derivatives from Salvia officinalis. Phytochemistry. 1999; 51:91–94.
37. Pearce AN, et al. Orthidines A-E, tubastrine, 3,4-dimethoxyphenethyl-β-guanidine, and 1,14-sperminedihomovanillamide: potential anti-inflammatory alkaloids isolated from the New Zealand ascidian Aplidium orthium that act as inhibitors of neutrophil respiratory burst. Tetrahedron. 2008; 64:5748–5755.
38. Sagawa T, et al. Cyclobutane dimers from the Colombian medicinal plant Achyrocline bogotensis. J Nat Prod. 2005; 68:502–505. [PubMed: 15844937]

39. Watanabe K, et al. Sarusubine A, a new dimeric Lythraceae alkaloid from Lagerstroemia subcostata. Tetrahedron Letters. 2007; 48:7502–7504.

40. Chen D, et al. A nonpeptidic agonist of glucagon-like peptide 1 receptors with efficacy in diabetic db/db mice. Proc Natl Acad Sci U S A. 2007; 104:943–948. [PubMed: 17213311]

41. Hockemeyer J, Burbiel JC, Mueller CE. Multigram-Scale Syntheses, Stability, and Photoreactions of A2A Adenosine Receptor Antagonists with 8-Styrylxanthine Structure: Potential Drugs for Parkinson's Disease. J Org Chem. 2004; 69:3308–3318. [PubMed: 15132536]

42. Liu Q, et al. Cyclobutane derivatives as novel nonpeptidic small molecule agonists of glucagon-like peptide-1 receptor. J Med Chem. 2012; 55:250–67. [PubMed: 22103243]

43. Fernandez D, Torres E, Aviles FX, Ortuno RM, Vendrell J. Cyclobutane-containing peptides: evaluation as novel metallocarboxypeptidase inhibitors and modelling of their mode of action. Bioorg Med Chem. 2009; 17:3824–8. [PubMed: 19414265]

44. Norris JD, et al. The homeodomain protein HOXB13 regulates the cellular response to androgens. Mol Cell. 2009; 36:405–16. [PubMed: 19917249]

45. Cesarone CF, Bolognesi C, Santi L. Improved microfluorometric DNA determination in biological material using 33258 Hoechst. Anal Biochem. 1979; 100:188–97. [PubMed: 94515]

46. Norris JD, et al. The homeodomain protein HOXB13 regulates the cellular response to androgens. Mol Cell. 2009; 36:405–16. [PubMed: 19917249]

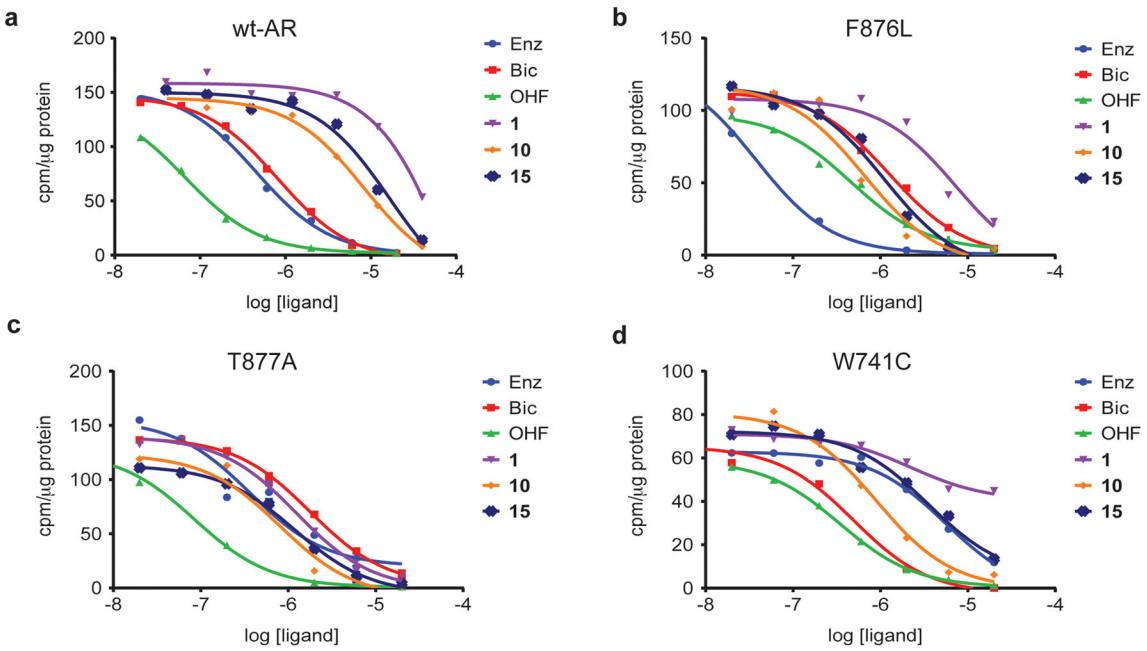

Figure 1. CBs compete with androgen binding to AR

HEK293 cells were transfected with vectors expressing (**a**) wt-AR (**b**) F876L (**c**) T877A or (**d**) W741C and duplicate wells were incubated for 2 hours with ^{3}H-R1881 plus increasing doses of **1**, **10**, and **15**. Scintillation counting was used to measure bound R1881 and total protein was used to normalize cell number. Experiment was performed in triplicate and a representative experiment is shown.

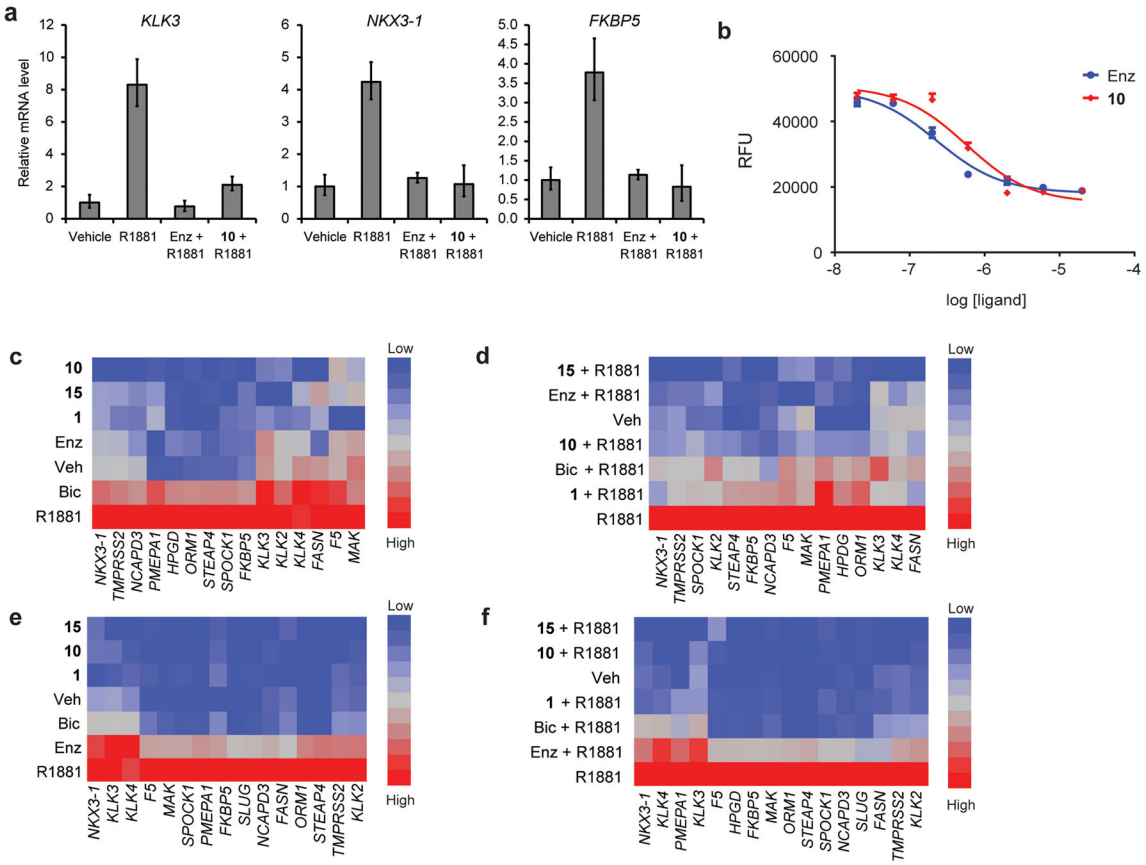

Figure 2. CBs inhibit AR activity in models of CRPC

(**a**) LNCaP cells were treated with vehicle, R1881 (0.1 nM), Enz (5 μM) + R1881 (0.1 nM), or **10** (5 μM) + R1881 (0.1 nM). Real-time PCR was used to assess AR target gene expression. Error bars represent s.d. of triplicate wells from a representative experiment performed in triplicate. (**b**) LNCaP cells were treated with R1881 (0.1 nM) and increasing concentrations of Enz or **10**. Cell growth was determined after 7 days by measuring DNA content using Hoechst dye. Error bars represent s.d. of triplicate wells from a representative experiment performed in triplicate. Real-time PCR analysis was used to assess AR target gene expression in LNCaP-AR cells treated with **1**, **10**, **15** (20 μM), Enz (10 μM), or Bic (10 μM) in the (**c**) absence or (**d**) presence of R1881 (0.1 nM). Heatmaps were generated from real-time PCR data after analysis with JMP pro software (SAS) using the Ward hierarchical clustering algorithm. Experiments were performed in duplicate and a representative experiment is shown (**e**) and (**f**) same as in (**c**) and (**d**) except for activity in LNCaP-F876L cells was measured.

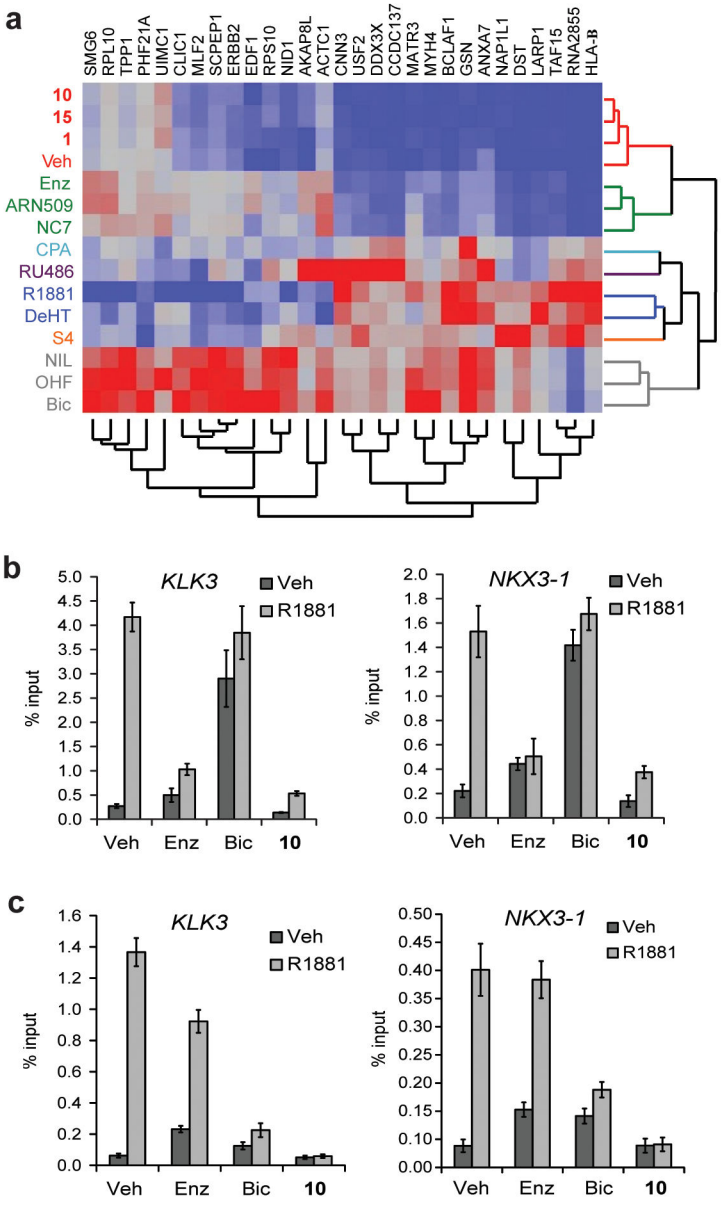

Figure 3. CBs are mechanistically distinct antiandrogens

(**a**) **1**, **10**, and **15** induce a novel conformation in AR. Interaction profiles of AR ligands and vehicle control (veh) were generated using 29 AR cofactors. Profiles were analyzed using Ward hierarchical clustering and the resulting dendogram and heatmap represent the structural relationships between the seven clusters (agonists and partial agonists, blue and orange; CPA and RU 486, light blue and purple; enzalutamide and related structures, green; antagonists with partial agonist activity, grey; apo, red). (**b** and **c**) **10** inhibits binding of AR to DNA in models of CRPC. LNCaP-AR (**b**) or LNCaP-F876L (**c**) cells were treated with Enz (10 μM), Bic (10 μM), or **10** (20 μM) in the absence or presence of R1881 (LNCaP-AR, 0.1 nM; LNCaP-F876L, 0.3 nM) and chromatin immunoprecipitation was performed to assess the recruitment of AR to target gene promoters by real-time PCR. Error bars in **b** and **c** represent s.d. of triplicate wells from a representative experiment performed in duplicate.

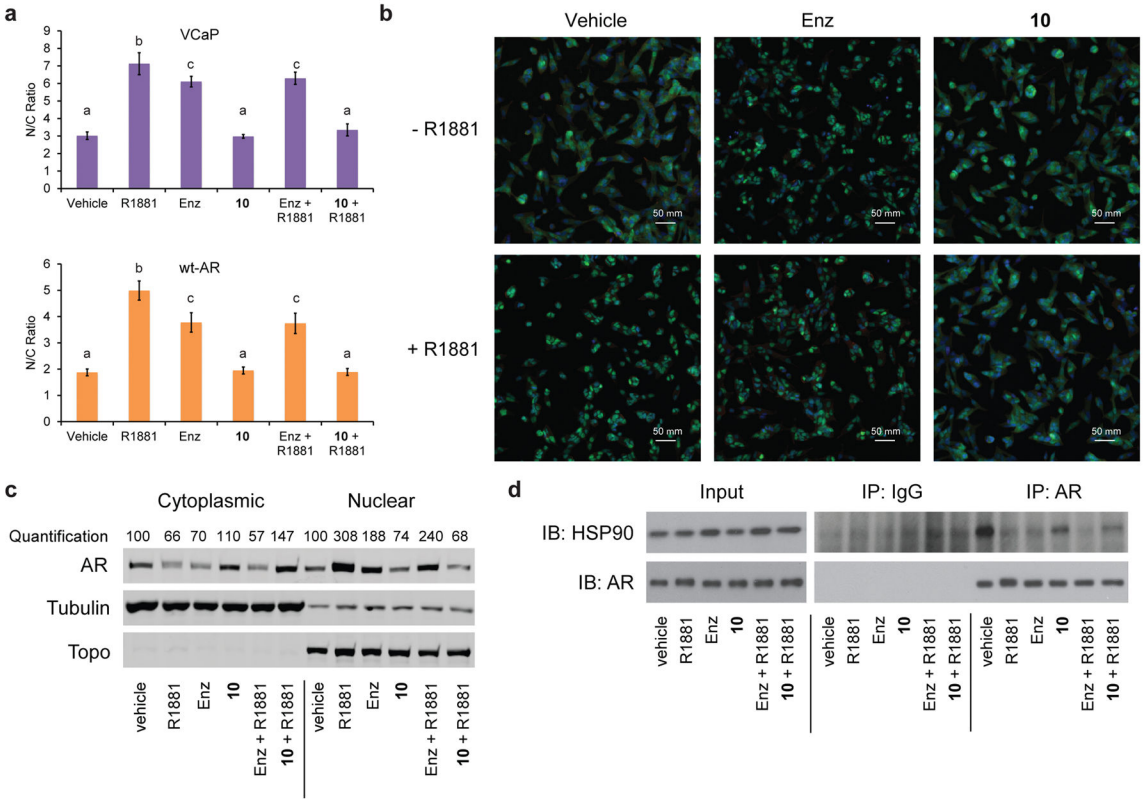

Figure 4. 10 inhibits nuclear localization of AR

(**a–c**) **10** does not promote nuclear accumulation of AR. (**a**) VCaP cells (top) or HEK293 cells transfected with a vector expressing wt-AR (bottom) were treated with R1881 (0.1 nM), Enz (20 μM), or **10** (20 μM) as indicated. Cells were stained for AR, DAPI, and Phalloidin and N/C ratios were quantified using high content imaging (ArrayScan). Error bars represent s.e.m. from 5 independent experiments. Letters indicate statistically similar groups ($p < 0.05$) as determined by one-way ANOVA analysis followed by Bonferroni multiple comparison test. (**b**) Representative fluorescence microscopy images from an ArrayScan experiment with VCaP cells after indicated treatments; AR (green), DAPI (blue), and Phalloidin (red). (**c**) HEK293 cells expressing wt-AR were treated with indicated ligands for 4 hours prior to fractionation into nuclear and cytoplasmic compartments. Proteins were analyzed by infrared fluorescent imaging (LI-COR Odyssey) and AR levels were normalized to α-tubulin (cytoplasm) or topoisomerase (nucleus) and presented as percent relative to vehicle treatment. The experiment was performed in triplicate and a representative experiment is shown. Full gels in Supplementary Fig. 12. (**d**) **10** does not disrupt the interaction between HSP90 and AR. HEK293 cells were transfected with wt-AR expression vector and treated with the indicated ligands for 4 hours prior to immunoprecipitation using antiAR antibody. Immunoprecipitated proteins were assessed by western blotting using AR and HSP90 antibodies. The experiment was performed in triplicate and a representative experiment is shown. Full gels in Supplementary Fig. 12.

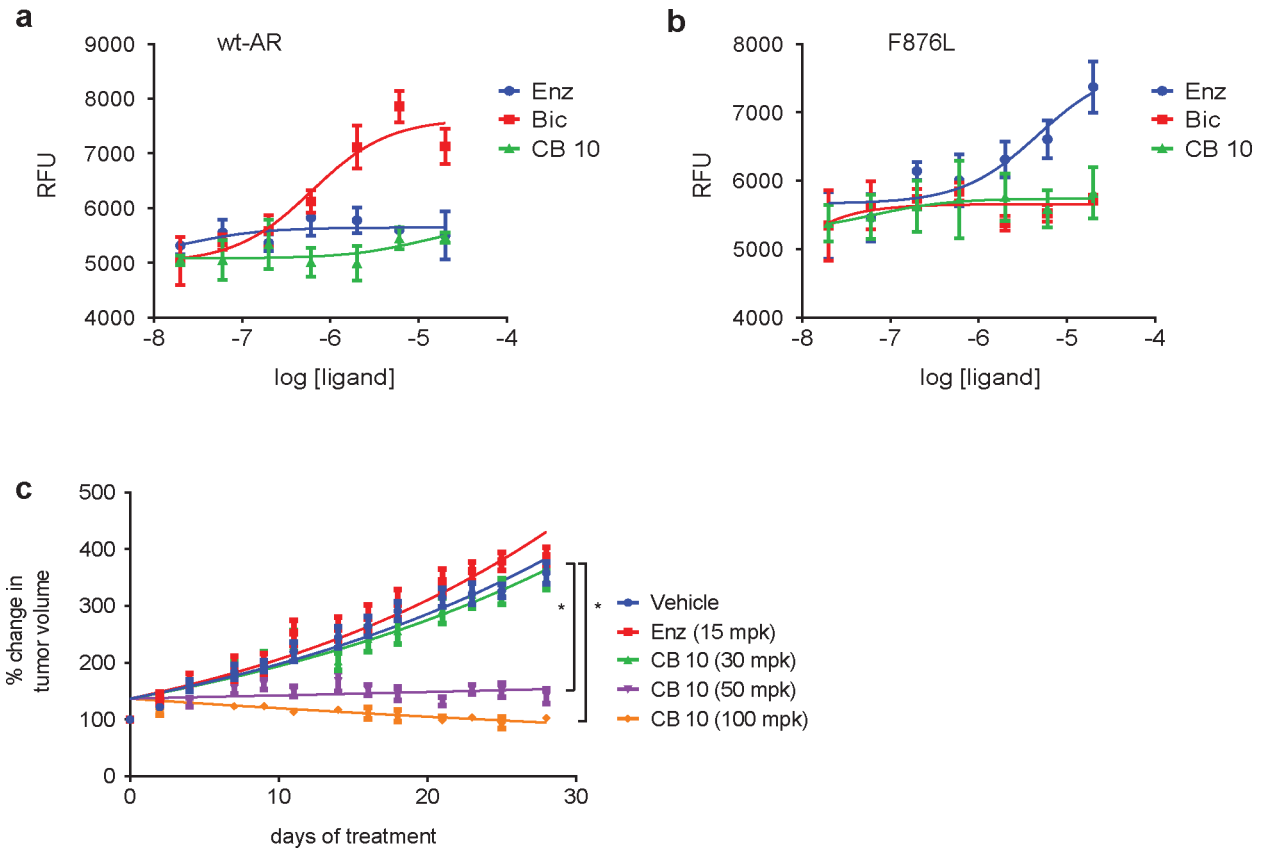

Figure 5. 10 does not promote cell growth in models of CRPC and inhibits tumor growth in a model of enzalutamide resistance

(**a**) LNCaP-AR or (**b**) LNCaP-F876L cells were treated for 7 days with increasing doses of Enz, Bic, or **10** and cell growth was assessed by measuring DNA content. Error bars indicate s.d. of triplicate samples from a representative experiment performed in duplicate. (**c**) LNCaP-F876L cells were implanted into the flank of castrated male NSG mice. When tumors reached ~0.1 cm^3 volume (4–5 weeks post-injection), mice (n = 13–14) were randomized to vehicle, Enz (15 mg/kg – MTD by this administration route), or **10** (30, 50, or 100 mg/kg). Tumor growth for each group is presented as average tumor volume +/− s.e.m. per study arm (N= 13 or 14) during 28 daily treatments. Only 50 and 100 mg/kg **10** arms differ significantly from the vehicle control in days 14–28 of treatment (2-way ANOVA followed by Bonferroni comparison, * $p < 0.0001$).